Journal of Solid State Chemistry 184 (2011) 2322–2328

Contents lists available at ScienceDirect

Journal of Solid State Chemistry

journal homepage: www.elsevier.com/locate/jssc

The crystal structure of $Yb_2(SO_4)_3 \cdot 3H_2O$ and its decomposition product, β-$Yb_2(SO_4)_3$

Stuart J. Mills [a,b,*], Václav Petříček [c], Anthony R. Kampf [b], Regine Herbst-Imer [d], Mati Raudsepp [a]

[a] Department of Earth and Ocean Sciences, University of British Columbia, Vancouver, British Columbia, Canada V6T 1Z4
[b] Mineral Sciences Department, Natural History Museum of Los Angeles County, 900 Exposition Boulevard, Los Angeles, California 90007, USA
[c] Institute of Physics, Academy of Sciences of the Czech Republic, v.v.i., Na Slovance 2, 182 21 Praha, Czech Republic
[d] Department of Structural Chemistry, University of Göttingen, Tammannstraße 4, 37077 Göttingen, Germany

ARTICLE INFO

Article history:
Received 20 February 2011
Received in revised form
3 June 2011
Accepted 20 June 2011
Available online 28 June 2011

Keywords:
Crystal structure
Hydrothermal synthesis
Rare earth
Sulphate
Ytterbium
Yttrium

ABSTRACT

$Yb_2(SO_4)_3 \cdot 3H_2O$, synthesised by hydrothermal methods at 220(2) °C, has been investigated by single crystal X-ray diffraction. $Yb_2(SO_4)_3 \cdot 3H_2O$ crystallises in space group $Cmc2_1$ and is isostructural with $Lu_2(SO_4)_3 \cdot 3H_2O$. The crystal structure has been refined to $R_1 = 0.0145$ for 3412 reflections [$F_o > 3\sigma(F)$], and 0.0150 for all 3472 reflections. The structure of $Yb_2(SO_4)_3 \cdot 3H_2O$ is a complex framework of YbO_6 octahedra, YbO_8 and $YbO_5(H_2O)_3$ polyhedra and SO_4 tetrahedra. Thermal data shows that $Yb_2(SO_4)_3 \cdot 3H_2O$ decomposes between 120 and 190 °C to form β-$Yb_2(SO_4)_3$. The structure of a twinned crystal of β-$Yb_2(SO_4)_3$ was solved and refined using an amplimode refinement in *R*3*c* with an $R_1 = 0.0755$ for 8944 reflections [$F_o > 3\sigma(F)$], and 0.1483 for all 16,361 reflections. β-$Yb_2(SO_4)_3$ has a unique structural topology based on a 3D network of pinwheels.

1. Introduction

There has been much interest over the years in the study of rare-earth element (REE) salts; however, there has been little focus on structural investigations of these phases. Of all the basic REE sulphates known, only the octahydrates, $REE_2(SO_4)_3 \cdot 8H_2O$, have been fully characterised [1–10]. Some crystal structure refinements are known for the nonahydrates (La and Ce) [8,9,11,12], pentahydrates (Nd and Ce) [8,13] and tetrahydrates (La, Ce, Nd, Tb and Er) [5,14,15] and one trihydrate is known (Lu) [8]. No mono- or dihydrates have so far been reported. Thermal data is also lacking for most of these compounds.

The interest in the octahydrate compounds arose from an erroneous structure determination for the Pr-analogue [9] and its supposed pyroelectricity. Subsequent analyses showed it to be isostructural with all other $REE_2(SO_4)_3 \cdot 8H_2O$ (e.g. [3]) and then remaining REE octahydrate analogues were then synthesised for completion [10]. The REE ions have different coordination environments in the different hydrates—in octahydrates and pentahydrates they are in 8-fold coordination [1–10]; in enneahydrates they are in 8- and 9-fold coordination [8,9,11,12]; in tetrahydrates they are in 7- and 8-fold coordination [5,14,15]; whilst in trihydrates they are in 6- and 8-fold coordination [8]. Here we report the crystal structure of $Yb_2(SO_4)_3 \cdot 3H_2O$ and its decomposition product, β-$Yb_2(SO_4)_3$.

2. Experimental

2.1. Synthesis of $Yb_2(SO_4)_3 \cdot 3H_2O$

$Yb_2(SO_4)_3 \cdot 3H_2O$ was synthesised under mild hydrothermal conditions in Teflon-lined stainless steel autoclaves. The crystals were grown by mixing 0.4 g of reagent grade (Alfa, 99.9% purity) Yb_2O_3 with 1.9 g of H_2SO_4 (as an 85% aqueous solution) and 12.8 g of distilled water, so that the autoclaves were filled to 50% of their inner volume. The mixture was kept at 220(2) °C under autogeneous pressure for 400 h. The autoclaves were then slowly cooled from 220 °C to room temperature over 24 h. At the end of the reaction, all of the water had evaporated and a mat of transparent, colourless crystals lined the bottom of the autoclave. No other phases were observed in bulk PXRD diffractograms.

2.2. Formation of β-$Yb_2(SO_4)_3$

β-$Yb_2(SO_4)_3$ was formed by heating $Yb_2(SO_4)_3 \cdot 3H_2O$ crystals in an oven at 200(2) °C and 30(3)% relative humidity for 1 h in open air. The $Yb_2(SO_4)_3 \cdot 3H_2O$ crystals turned translucent and

* Corresponding author at: Geosciences, Museum Victoria, GPO Box 666, Melbourne 3001, Australia. Tel.: +61 3 9270 5064; fax: +61 3 9270 5043.
E-mail address: smills@museum.vic.gov.au (S.J. Mills).

0022-4596/$ - see front matter © 2011 Elsevier Inc. All rights reserved.
doi:10.1016/j.jssc.2011.06.018

their colour changed from colourless to off-white with a yellowish hue.

2.3. Thermogravimetric analysis

TGA analyses were obtained from 38.32 mg of $Yb_2(SO_4)_3 \cdot 3H_2O$. The sample was analysed using a Perkin Elmer Pyris 6 TGA (Department of Chemistry, University of British Columbia) over the temperature range 50–900 °C, with a heating rate of 5 °C/min between 50 and 400 °C and 10 °C/min between 400 and 900 °C.

2.4. X-ray diffraction

2.4.1. $Yb_2(SO_4)_3 \cdot 3H_2O$

The single-crystal study was completed using a Bruker X8 Apex II single-crystal diffractometer at the Department of Chemistry, University of British Columbia. Irregular fragments of $Yb_2(SO_4)_3 \cdot 3H_2O$ and β-$Yb_2(SO_4)_3$ with the dimensions $135 \times 95 \times 75$ and $75 \times 55 \times 50$ μm, respectively, were used for collection of intensity data at 293 K (Table 1). The intensity data were processed with the Bruker Apex programme suite, with data reduction using the SAINT programme [16] and absorption correction by the multi-scan method using SADABS [17]. No twinning was observed for $Yb_2(SO_4)_3 \cdot 3H_2O$.

The crystal structure of $Yb_2(SO_4)_3 \cdot 3H_2O$ was refined in space group $Cmc2_1$ (No. 36), using SHELXL-97 [18] with the starting coordinates of $Lu_2(SO_4)_3 \cdot 3H_2O$ [8]. In the latter stages of the refinement, large thermal parameters indicated that W2 and W3 were split. Subsequent iterations showed that these split sites were fully occupied. The final model for the refinement converged to $R_1 = 0.0145$ for 3412 reflections [$F_o > 3\sigma(F)$], and 0.0150 for all 3472 reflections.

2.4.2. β-$Yb_2(SO_4)_3$

The diffraction pattern of the β-$Yb_2(SO_4)_3$ exhibited some very interesting features. All sharp diffraction spots can be indexed in a *P*-centred pseudo-cubic cell with $a \sim 12.8$ Å and angles that deviated away from 90° [$\alpha = 90.065(2)$, $\beta = 90.055(2)$ and $\gamma = 90.014(2)$°]. The R_{int} for the highest Laue symmetry compatible with the pseudo-cubic cell, i.e. $G = m\bar{3}m$, (lattice point group) gives a very high R_{int} of 19.4% for observed reflections ($I > 3\sigma(I)$). Similarly for all subgroups of the lattice point group, except for monoclinic $2/m$ (directed along one of pseudo-cubic axes), the R_{int} is also very high (~15%). This means that the structure symmetry is either monoclinic or the sample is a twin, with volume fractions significantly deviated from the uniform distribution. The second possibility generally allows for higher symmetry, but averaging has to be carefully checked. Possible diffraction symmetry of twins has been discussed for example in [19], where it has been shown that the symmetry element of the chosen subgroup *H* can be used for averaging process only if conjugated elements ghg^{-1} for all $g \in G$ are elements of *H*. This also means that the diffraction pattern has a full symmetry of *H* if it is a normal subgroup of *G*. The highest symmetrical candidates of *G* are thus $4/mmm$ and $\bar{3}m$. While the tetragonal space group contains the subgroup *mmm* (being invariant in the sense mentioned above), it similarly gives a high R_{int} of 15%. On the other hand, averaging in $\bar{3}m1$ and taking into account twinning give a R_{int} of 4.85%.

Another interesting feature of the diffraction pattern is that after transforming reflections from the pseudo-cubic cell into the trigonal cell, all strong reflections (main reflections) fulfil the conditions $h = 2n$ and $k = 2n$. In accordance with modulated structures, we shall call them main reflections and the remaining ones satellite reflections. This allows us to solve first an average structure in a smaller cell and then complete it either by expanding the solution into the supercell and refining a model randomly displaced, or using 5*d*

Table 1
Crystallographic information for $Yb_2(SO_4)_3 \cdot 3H_2O$ and β-$Yb_2(SO_4)_3$.

Crystal data		
Formula	**$Yb_2(SO_4)_3 \cdot 3H_2O$**	**$Yb_2(SO_4)_3$**
Cell parameters		
a (Å)	13.5536(11)	18.1958(4)
b (Å)	18.4678(17)	18.1958(4)
c (Å)	9.2509(8)	22.2853(5)
V (Å^3)	2315.5(3)	6400.9(8)
Z	8	24
Angles (°)	90, 90, 90	90, 90, 120
Space group	$Cmc2_1$	*R*3*c*
Data collection		
Temperature (K)	293(2)	293(2)
λ (Mo*K*α)	0.71073	0.71073
Crystal size	$135 \times 95 \times 75$ μm	$75 \times 55 \times 50$ μm
2θ max. (°)	60.98	84.54
Reflection range	$-19 \le h \le 6$; $-26 \le k \le 26$; $-13 \le l \le 13$	$-34 \le h \le 34$; $-29 \le k \le 34$; $-41 \le l \le 36$
Total no. reflections	13,428	50,047
No. unique reflections	3472	16,361
No. reflections, $F > 3\sigma(F)$	3412	8944
Absorption correction (mm^{-1})	$\mu = 16.683$	$\mu = 12.066$
R_{merg} on F^2	0.0228	0.0335
Refinement		
No. parameters refined	202	768
R_1, $F > 3\sigma(F)$	0.0145	0.0755
R_1, all data	0.015	0.1483
wR_2 (F^2), all data	0.0293[a]	0.0812[b]
GOF	1.072	2.15
$\Delta\sigma_{min}$, $\Delta\sigma_{max}$ (e/Å^3)	−0.735, 1.314	−0.93, 1.25

[a] $w = 1/[\sigma^2(F_o^2) + (0P^2 + 0.5637P)]$, $P = [2F_c^2 + \mathrm{Max}(F_o^2, 0)]/3$.
[b] $1/w = \sigma^2(F) + (0.01F)^2$.

superspace approach or applying an amplimode refinement. Note that presence of two modulation vectors (1/2,0,0) and (0,1/2,0) makes it impossible to use 4*d* superspace unless the point group $\bar{3}m$ is reduced to *m* and additional twinning is introduced.

The solution of the average structure was first modelled in space group *P*-1 (No. 2) by transforming the orthorhombic structure of $Y_2(SO_4)_3$ [20] to triclinic using TRANSTRU from the Bilbao Crystallographic Server [21], and then refining the atom positions. The final refinement, which included several twin individuals, refined to $R_1=0.0960$ for 3061 reflections [$F_o > 3\sigma(F)$], with all atoms located.

A subsequent refinement in $R\bar{3}m$ (No. 166) is as a four-fold twin with the twinning matrices:

$$\mathbf{T}_1=\begin{bmatrix}1&0&0\\0&1&0\\0&0&1\end{bmatrix} \qquad \mathbf{T}_2=\begin{bmatrix}1/3&2/3&-4/3\\-1/3&1/3&-8/3\\-1/3&1/3&1/3\end{bmatrix}$$

$$\mathbf{T}_3=\begin{bmatrix}1/3&0&-8/3\\2/3&-1&-4/3\\-1/3&0&-1/3\end{bmatrix} \qquad \mathbf{T}_4=\begin{bmatrix}1&-2/3&-4/3\\1&-1/3&4/3\\0&-1/3&1/3\end{bmatrix}$$

Table 2
Atomic positions and displacement parameters.

atom	*x*	*y*	*z*	U_{eq}	U_{11}	U_{22}	U_{33}	U_{23}	U_{13}	U_{12}
(a) $Yb_2(SO_4)_3\cdot 3H_2O$										
Yb1	0.0	0.371241(9)	0.49989(2)	0.00761(4)	0.00658(9)	0.00789(8)	0.00837(7)	−0.00029(6)	0.0	0.0
Yb2	0.5	0.393394(9)	0.505950(15)	0.00665(4)	0.00494(9)	0.00755(8)	0.00746(7)	0.00045(7)	0.0	0.0
Yb3	0.297690(10)	0.152643(7)	0.540027(19)	0.01041(4)	0.00899(7)	0.01181(6)	0.01043(5)	0.00049(5)	−0.00052(5)	−0.00289(5)
S1	0.25155(6)	0.34165(4)	0.43078(8)	0.01004(16)	0.0057(5)	0.0136(4)	0.0108(3)	0.0003(3)	−0.0018(3)	−0.0015(3)
O11	0.2536(3)	0.26831(15)	0.4852(4)	0.0428(10)	0.040(2)	0.0151(13)	0.073(3)	0.0147(16)	0.0123(17)	0.0043(14)
O12	0.1646(2)	0.37787(15)	0.4921(5)	0.0303(7)	0.0074(15)	0.0268(14)	0.057(2)	−0.0112(14)	0.0026(16)	−0.0011(11)
O13	0.3382(2)	0.38180(15)	0.4810(4)	0.0239(7)	0.0042(14)	0.0285(14)	0.039(2)	−0.0134(12)	−0.0026(12)	−0.0053(10)
O14	0.2501(4)	0.3425(3)	0.2769(4)	0.0573(14)	0.054(4)	0.111(4)	0.0075(15)	0.0039(17)	−0.0078(15)	−0.024(2)
S2	0.0	0.25278(6)	0.22259(11)	0.0088(2)	0.0122(7)	0.0075(5)	0.0069(4)	−0.0009(3)	0.0	0.0
O21	0.0	0.2667(2)	0.3795(4)	0.0277(11)	0.062(4)	0.0127(18)	0.0082(15)	−0.0053(13)	0.0	0.0
O22	0.0	0.1750(2)	0.2036(4)	0.0338(12)	0.081(4)	0.0078(17)	0.0120(16)	−0.0021(13)	0.0	0.0
O23	−0.0864(3)	0.2826(3)	0.1606(4)	0.0593(13)	0.051(3)	0.081(3)	0.046(2)	0.023(2)	−0.0102(18)	0.042(2)
S3	0.5	0.50235(8)	0.26752(11)	0.0120(2)	0.0175(6)	0.0102(4)	0.0084(4)	0.0021(4)	0.0	0.0
O31	0.5	0.42249(17)	0.2536(3)	0.0155(8)	0.025(2)	0.0087(15)	0.0134(14)	0.0017(12)	0.0	0.0
O32	0.5	0.51531(19)	0.4247(4)	0.0225(9)	0.045(3)	0.0138(18)	0.0087(14)	0.0001(12)	0.0	0.0
O33	0.5860(2)	0.53489(14)	0.1958(3)	0.0181(5)	0.0168(16)	0.0175(12)	0.0201(12)	0.0058(10)	0.0030(10)	−0.0019(10)
S4	0.5	0.21418(6)	0.32561(11)	0.0084(2)	0.0108(6)	0.0082(5)	0.0060(4)	−0.0008(3)	0.0	0.0
O41	0.5	0.28889(19)	0.3781(4)	0.0204(9)	0.035(3)	0.0079(16)	0.0178(16)	−0.0025(13)	0.0	0.0
O42	0.5	0.2150(2)	0.1647(4)	0.0345(13)	0.081(4)	0.020(2)	0.0030(15)	−0.0008(13)	0.0	0.0
O43	0.4118(3)	0.17700(18)	0.3693(3)	0.0335(8)	0.022(2)	0.0353(18)	0.0426(18)	−0.0161(15)	0.0177(13)	−0.0146(14)
S5	0.0	0.45959(6)	0.15919(11)	0.0110(2)	0.0126(7)	0.0074(5)	0.0129(5)	0.0023(4)	0.0	0.0
O51	0.0	0.4395(2)	0.3105(4)	0.0351(13)	0.069(4)	0.023(2)	0.0127(17)	0.0090(16)	0.0	0.0
O52	0.0	0.5393(2)	0.1507(4)	0.0262(11)	0.055(3)	0.0119(18)	0.0122(16)	0.0031(14)	0.0	0.0
O53	0.0867(3)	0.4328(2)	0.0894(5)	0.0630(14)	0.061(3)	0.040(2)	0.088(3)	0.019(2)	0.053(2)	0.0268(19)
W1	0.1238(2)	0.15858(16)	0.5478(5)	0.0350(7)	0.0116(16)	0.0367(15)	0.057(2)	0.0149(15)	0.0008(17)	−0.0058(13)
W2*a*[a]	0.2303(7)	0.1441(4)	0.3054(7)	0.0287(15)						
W2*b*[a]	0.2509(6)	0.1095(5)	0.3132(10)	0.041(2)						
W3*a*[a]	0.2417(6)	0.0348(4)	0.5858(9)	0.0393(16)						
W3*b*[a]	0.2273(5)	0.0372(3)	0.5133(8)	0.0276(12)						
(b) β-$Yb_2(SO_4)_3$										
Atom	*x*	*y*	*z*	U_{iso}						
Yb11	0.0	0.0	0.153485	0.0121(6)						
Yb12	−0.49913(8)	−0.00638(7)	0.13397(10)	0.0121(6)						
Yb13	0.0	0.0	0.87434(13)	0.0121(6)						
Yb14	−0.50254(10)	−0.00723(6)	0.85675(7)	0.0121(5)						
S11	−0.9919(4)	−0.1387(4)	0.2636(3)	0.0102(14)						
S12	−0.4992(5)	−0.1481(4)	0.2487(3)	0.0102(12)						
S13	−0.9900(4)	−0.6316(4)	0.2532(3)	0.0102(15)						
S14	−0.5023(5)	−0.6313(4)	0.2508(3)	0.0102(12)						
O11	−0.0028(15)	−0.1003(15)	0.2065(9)	0.026(5)						
O12	−0.5222(16)	−0.1135(14)	0.1981(9)	0.026(5)						
O13	−0.0039(14)	−0.6074(14)	0.1936(10)	0.026(5)						
O14	−0.5234(15)	−0.5958(15)	0.1981(9)	0.026(5)						
O15	−0.9603(15)	−0.8955(12)	0.8027(8)	0.026(4)						
O16	−0.4717(13)	−0.9089(13)	0.7954(8)	0.026(5)						
O17	−0.9536(13)	−0.3729(14)	0.8075(9)	0.026(5)						
O18	−0.5059(15)	−0.4003(15)	0.7982(10)	0.026(5)						
O21	−0.0054(12)	−0.9019(13)	0.0912(7)	0.013(4)						
O22	−0.4627(10)	−0.8704(11)	0.1180(7)	0.013(3)						
O23	−0.9839(12)	−0.3772(12)	0.0921(7)	0.013(4)						
O24	−0.4901(12)	−0.3815(12)	0.0938(7)	0.013(4)						
O25	−0.0549(12)	−0.1328(11)	0.8943(7)	0.013(4)						
O26	−0.5113(12)	−0.0958(12)	0.9221(7)	0.013(4)						
O27	−0.0019(13)	−0.5930(12)	0.9131(8)	0.013(4)						
O28	−0.5114(12)	−0.5960(12)	0.9168(8)	0.013(4)						

[a] Each split water site has 0.5 occupancy.

converged to $R_1=0.0539$ for 1855 unique observed reflections. The relevant twinning fractions are 0.351(3), 0.148(2), 0.353(2) and 0.148(2), respectively. These values are strongly deviated from the uniform domain distribution as predicted.

All the three methods mentioned above were used to get a full description of the supercell. It has been found that the correct supercell space group is the non-cetrosymmetric space group *R*3*c* (No. 161). For the commensurate model we have used the superspace group *X*3*c* (α,0,0)00(0,α,0)00 with *X*={(0,0,0,0,0),(2/3,1/3,1/3,1/3,2/3),(1/3,2/3,2/3,2/3,1/3)} and $\alpha=1/2$. Then the **t** section $(1/3,-1/3)$ generates the supercell symmetry *R*3*c*. Both refinements gave identical results.

The third method, based on using amplimodes, seems to be a very elegant, time efficient and promising approach for handling simple commensurate cases such as this. There is no need to introduce a more complicated description in 5*d* superspace, but it still makes it possible to start with some dominating distortions and using a step-by-step approach to reach a final solution. This method is based on symmetry-mode analysis of distorted structures (e.g. [22,23]) and its application to crystallography [24]. The starting model, as obtained from the Bilbao Crystallographic Server [21], has been used as an input to the new version of the programme Jana2006 [25]. The structure has been successfully refined and it gives identical results as two previously mentioned methods. The magnitudes of displacive distortions as defined in [21] for individual atoms of the parent structure in Å are

	Yb1	S1	O1	O2
Γ_1^+	0.0142(12)	0.021(10)	0.41(4)	0.44(3)
Γ_2^-	0.0	0.633(19)	0.58(6)	0.92(5)
F_1^+	0.060(2)	0.221(17)	1.38(5)	1.37(5)
F_2^-	0.6933(12)	0.893(12)	2.06(4)	2.45(4)

The refined atomic coordinates, site occupancies and displacement parameters for both compounds are given in Table 2 and polyhedral bond distances in Table 3. It should be noted that several crystals of β-$Yb_2(SO_4)_3$ were examined and all showed the same features and twinning noted above.

3. Results and discussion

3.1. Crystal structure of $Yb_2(SO_4)_3\cdot 3H_2O$

The crystal-structure determination shows that $Yb_2(SO_4)_3\cdot 3H_2O$ is isostructural with $Lu_2(SO_4)_3\cdot 3H_2O$ [8]—the only other known REE sulphate trihydrate. The structure of $Yb_2(SO_4)_3\cdot 3H_2O$ is a complex framework of YbO_6 octahedra, YbO_8 and $YbO_5(H_2O)_3$ polyhedra and SO_4 tetrahedra (Fig. 1). In this framework, none of the Yb polyhedra share elements with one another, rather they are linked via SO_4 tetrahedra. The most tightly bonded fragment of the framework is an unusual zig-zag chain of edge-sharing YbO_8 (Yb2) polyhedra and SO_4 (S3) tetrahedra parallel to *c* (Fig. 2). Another interesting type of linkage in the structure involves triple SO_4 tetrahedral links between opposing faces of Yb polyhedra. Such linkages exist between Yb1 and Yb2, between Yb2 and Yb3 and between Yb3 and Yb3 polyhedra. These triple linkages create a polyhedral cluster (Fig. 3) peripheral to the edge-sharing chain. Note that the Yb2 polyhedron in this cluster also participates in the edge-sharing chain. All other linkages between Yb polyhedra in the framework are via single SO_4 tetrahedra. The only unshared polyhedral vertices correspond to the three H_2O ligands of the Yb3 polyhedron.

The average bond lengths for the Yb polyhedra are ⟨^{VI}Yb1–O⟩ 2.204, ⟨^{VIII}Yb2–O⟩ 2.333 and ⟨^{VIII}Yb3–O⟩ 2.302 Å. The bond lengths appear to be typical for Yb in octahedral [26,27] or 8-fold coordination [28]. Interestingly, in the $YbO_5(H_2O)_3$ polyhedra, the shortest bonds are all to O atoms (2.25–2.28 Å), whereas the longer bonds are to the split water molecules (2.33–2.36 Å). Conversely, due to the connectivity of the structure, some of the SO_4 tetrahedra exhibit shortened apical bonds in order to connect with the shortest Yb–O bonds. The average bond lengths for the SO_4 tetrahedra are ⟨S1–O⟩ 1.451, ⟨S2–O⟩ 1.438, ⟨S3–O⟩ 1.473, ⟨S4–O⟩ 1.456 and ⟨S5–O⟩ 1.455 Å (Table 3). S3, the only tetrahedron that is edge-sharing with a Yb polyhedron, is the only SO_4 tetrahedra which is regular (i.e. with a S–O ~ 1.47 Å [29]).

Table 3
Polyhedral bond lengths (Å).

(a) $Yb_2(SO_4)_3\cdot 3H_2O$						
Yb1	O52	2.162(3)		S1	O14	1.424(3)
Yb1	O51	2.159(4)		S1	O11	1.445(3)
Yb1	O42	2.204(4)		S1	O13	1.464(3)
Yb1	O21	2.228(4)		S1	O12	1.469(3)
Yb1	O12	2.236(3)				
Yb1	O12	2.236(3)		⟨S1–O⟩		1.451
⟨Yb1–O⟩		2.204		S2	O23	1.415(3)
				S2	O23	1.415(3)
Yb2	O13	2.216(3)		S2	O22	1.446(4)
Yb2	O13	2.216(3)		S2	O21	1.474(4)
Yb2	O22	2.222(4)				
Yb2	O41	2.264(3)		⟨S2–O⟩		1.438
Yb2	O32	2.374(4)				
Yb2	O31	2.395(3)		S3	O33	1.470(3)
Yb2	O33	2.490(3)		S3	O33	1.470(3)
Yb2	O33	2.490(3)		S3	O32	1.473(3)
				S3	O31	1.480(4)
⟨Yb2–O⟩		2.333				
				⟨S3–O⟩		1.473
Yb3	O43	2.256(3)				
Yb3	O23	2.268(3)		S4	O43	1.436(3)
Yb3	O53	2.270(3)		S4	O43	1.436(3)
Yb3	O11	2.275(3)		S4	O41	1.463(4)
Yb3	O14	2.286(3)		S4	O42	1.489(4)
Yb3	W2B	2.333(9)				
Yb3	W3A	2.344(8)		⟨S4–O⟩		1.456
Yb3	W3B	2.349(6)				
Yb3	W2A	2.360(7)		S5	O53	1.429(4)
Yb3	W1	2.360(3)		S5	O53	1.429(4)
				S5	O51	1.448(4)
⟨Yb3–O⟩		2.302		S5	O52	1.474(4)
				⟨S5–O⟩		1.445
(b) β-$Yb_2(SO_4)_3$						
Yb11	O11	2.15(2)	×3	S11	O22	1.448(15)
Yb11	O21	2.30(2)	×3	S11	O15	1.458(20)
				S11	O11	1.512(25)
⟨Yb11–O⟩		2.225		S11	O26	1.533(27)
Yb12	O14	2.146(20)		⟨S11-O⟩		1.488
Yb12	O24	2.222(16)				
Yb12	O23	2.225(23)		S12	O18	1.387(27)
Yb12	O22	2.247(20)		S12	O21	1.437(18)
Yb12	O12	2.280(24)		S12	O12	1.451(27)
Yb12	O13	2.400(27)		S12	O28	1.548(27)
⟨Yb12–O⟩		2.253		⟨S12–O⟩		1.456
Yb13	O25	2.15(2)	×3	S13	O23	1.368(16)
Yb13	O15	2.30(5)	×3	S13	O13	1.461(25)
				S13	O17	1.465(21)
⟨Yb13–O⟩		2.225		S13	O27	1.591(29)
Yb14	O16	2.093(21)		⟨S13–O⟩		1.471
Yb14	O27	2.114(24)				
Yb14	O26	2.118(20)		S14	O24	1.358(18)
Yb14	O28	2.191(16)		S14	O16	1.469(21)
Yb14	O18	2.206(20)		S14	O14	1.480(27)
Yb14	O17	2.255(27)		S14	O25	1.587(23)
⟨Yb14–O⟩		2.163		⟨S14-O⟩		1.474

3.2. Decomposition of $Yb_2(SO_4)_3 \cdot 3H_2O$ to β-$Yb_2(SO_4)_3$

The decomposition of $Yb_2(SO_4)_3 \cdot 3H_2O$ to β-$Yb_2(SO_4)_3$ is fairly straightforward. Decomposition begins at about 120 °C then proceeds smoothly until about 190 °C when β-$Yb_2(SO_4)_3$ is formed (Fig. 4). No steps are seen at 145 or 170 °C when the dihydrate or monohydrate would be expected to be stable. β-$Yb_2(SO_4)_3$ remains stable until about 830 °C where it slowly starts to decompose. Conversion of β-$Yb_2(SO_4)_3$ into other phases such as Yb_2O_3 (with the release of sulphur and oxygen as gas) occurs above 900 °C. The most likely reaction sequence is

$$\beta\text{-}Yb_2(SO_4)_3 \rightarrow Yb_2O_2(SO_4) + 2SO_2\uparrow + O_2\uparrow$$

$$Yb_2O_2(SO_4) \rightarrow Yb_2O_3 + SO_2\uparrow + \tfrac{1}{2}O_2\uparrow$$

This reaction sequence has been observed in several of the other octahydrates [30–33].

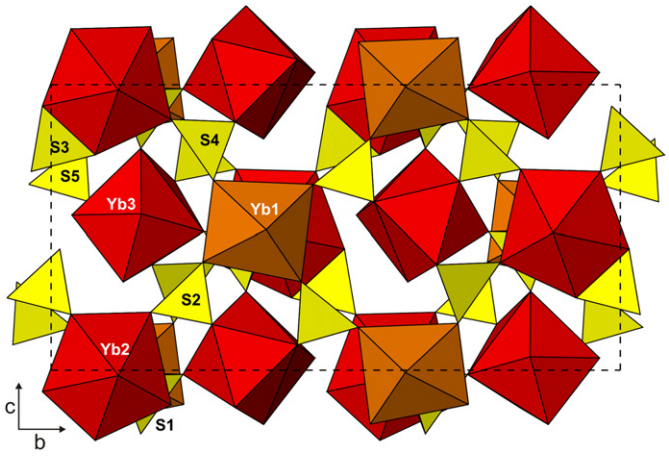

Fig. 1. Crystal structure framework of $Yb_2(SO_4)_3 \cdot 3H_2O$ viewed down *a*.

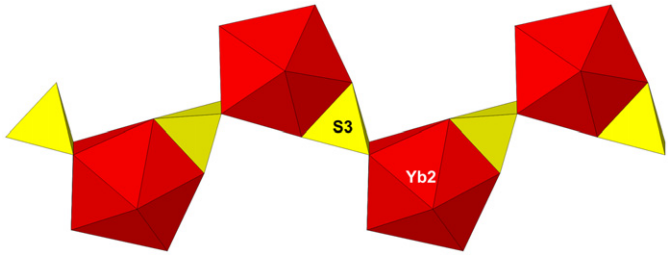

Fig. 2. Zig-zag chain of edge-sharing YbO_8 polyhedra and SO_4 tetrahedra in $Yb_2(SO_4)_3 \cdot 3H_2O$.

3.3. Crystal structure of β-$Yb_2(SO_4)_3$

The crystal structure of β-$Yb_2(SO_4)_3$ involves 4 independent Yb and 4 S atoms, which form YbO_6 octahedra and SO_4 tetrahedra. The structural topology is a unique 3D network of pinwheels

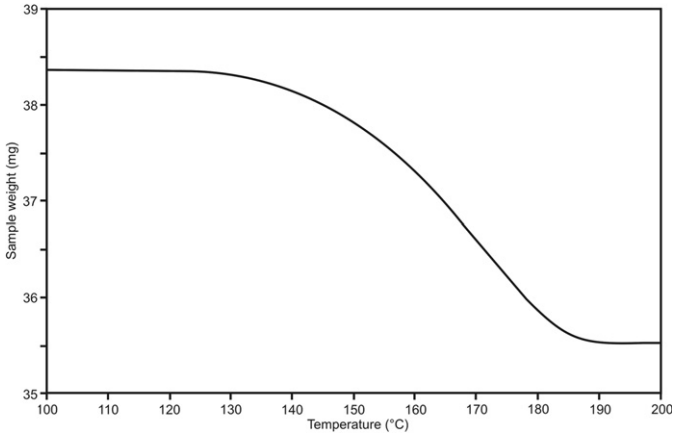

Fig. 4. Thermogravimetric results for $Yb_2(SO_4)_3 \cdot 3H_2O$.

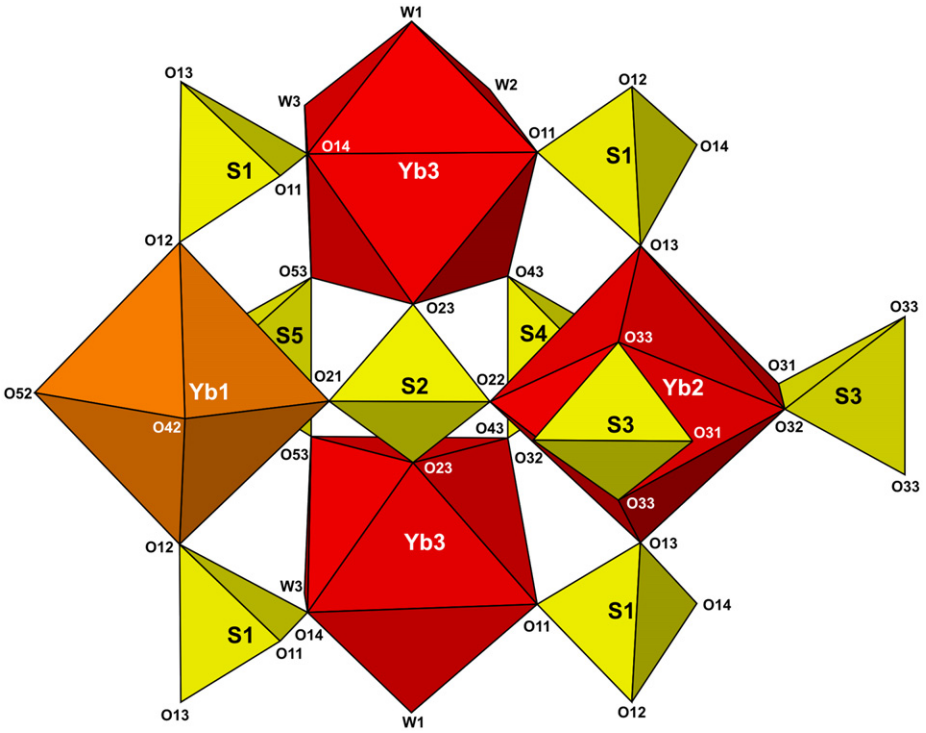

Fig. 3. Polyhedral cluster of SO_4 tetrahedra corner-sharing with Yb polyhedra in $Yb_2(SO_4)_3 \cdot 3H_2O$.

parallel to {0 0 1} (Fig. 5). Each YbO_6 octahedron has one SO_4 tetrahedron corner-connected to each oxygen atom. The pinwheel, as described by [34], is modified in β-$Yb_2(SO_4)_3$ such that instead of the tetrahedra pointing up or down they are twisted so that they can connect to other YbO_6 octahedra (Fig. 5) via tetrahedral linkages (see below). In other structures, the pinwheels are either condensed to form layers, such as those observed in merwinite or bracelets, and as those observed in glaserite [34], but in both cases the tetrahedra remain regular.

It is worth comparing the structure of β-$Yb_2(SO_4)_3$ with that of $Yb_2(SO_4)_3 \cdot 3H_2O$ in terms of linkages between octahedra via tetrahedra. As for $Yb_2(SO_4)_3 \cdot 3H_2O$, none of the Yb polyhedra share elements with one another, rather they are linked via SO_4 tetrahedra. However, in the structure of $Yb_2(SO_4)_3$ there is no edge-sharing between SO_4 tetrahedra and Yb octahedra. The triple SO_4 tetrahedral links between opposing faces of Yb polyhedra exist only between Yb11 and Yb13 and between Yb12 and Yb14 octahedra along [0 0 1]. Each of the YbO_6 octahedra links via double SO_4 tetrahedral links to three other YbO_6 octahedra forming sheets parallel to [0 0 1]. Although many intriguing structural fragments particularly involving the triple and double tetrahedral linkages could be noted, we have chosen the two pairs of triple-linked YbO_6 octahedra viewed down [1 1 0] with [0 0 1] vertical in Fig. 6.

Despite the slight distortion needed to maintain the connectivity, the average bond lengths for the YbO_6 octahedra appear fairly typical and consistent with those observed for $Yb_2(SO_4)_3 \cdot 3H_2O$ (Table 3). The SO_4 tetrahedra on the other hand are close to being perfectly regular for S13 and S14 and have mean average bond lengths about 1.47 Å (Table 3).

It is interesting to contrast the differences between the crystal-structure of β-$Yb_2(SO_4)_3$ and $Y_2(SO_4)_3$ [20]. Despite the closeness in ionic bonding of Y and Yb in solids, the topology of β-$Yb_2(SO_4)_3$ and $Y_2(SO_4)_3$ are different. We note that the crystallographic properties of Y are generally closer to Ho than Yb (e.g. [35]). In $Y_2(SO_4)_3$, the YO_6 octahedron has one triple SO_4 link to one other YO_6 octahedron and only two double links to two other YO_6

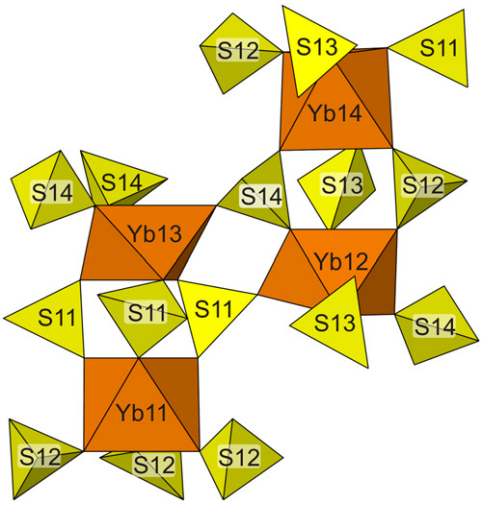

Fig. 6. Pairs of triple-linked YbO_6 octahedra viewed down [1 1 0] with [0 0 1] vertical in β-$Yb_2(SO_4)_3$.

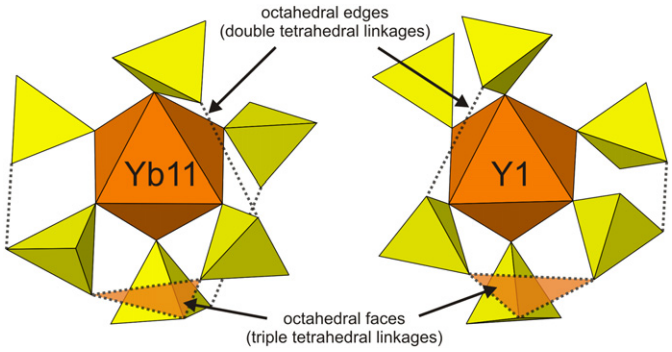

Fig. 7. Octahedral–tetrahedral linkages found in $Y_2(SO_4)_3$ (and $Er_2(SO_4)_3$) and β-$Yb_2(SO_4)_3$.

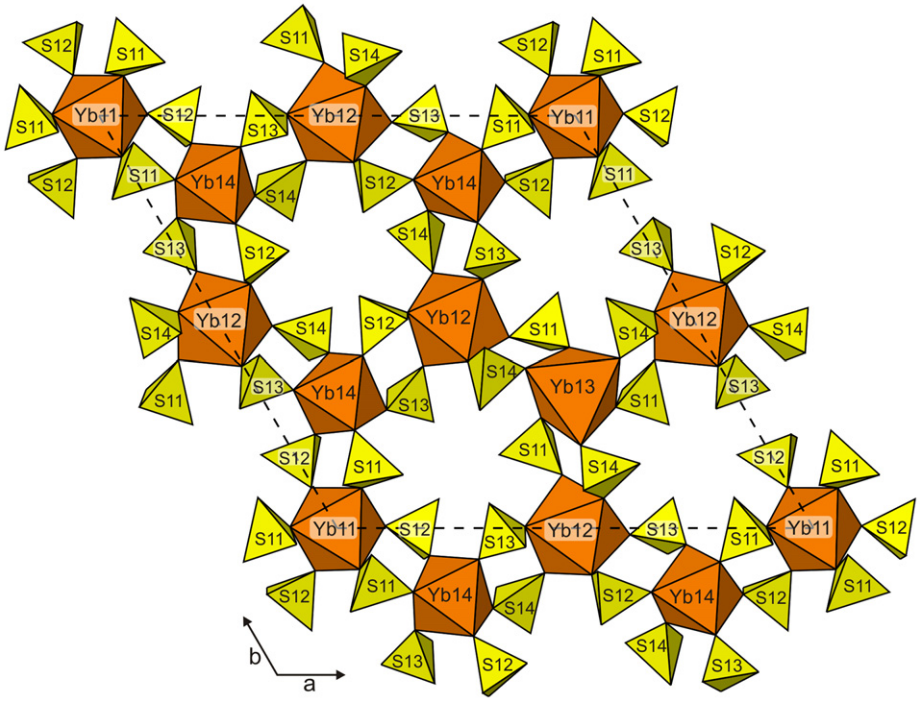

Fig. 5. Layer of pinwheels in β-$Yb_2(SO_4)_3$ parallel to {0 0 1}.

octahedra (Fig. 7). It is also interesting to note that in $Y_2(SO_4)_3$ the S–O bond lengths are on the order of 0.02 Å shorter than for β-$Yb_2(SO_4)_3$, which leaves the S atoms overbonded in the Y compound. It should be noted however that this value does not take into account the error in the bond lengths. The overbonding appears to have been transferred somewhat from the S atoms to the Yb in β-$Yb_2(SO_4)_3$ by the shortening of two of the Yb–O bonds. Nevertheless, it appears that the local bonding environments are complex and simple bond valence models might not be able to adequately describe them.

Only two other $REE_2(SO_4)_3$ phases have been previously reported. $Er_2(SO_4)_3$ was described by [36,37] and is isostructural with $Y_2(SO_4)_3$, while $Nd_2(SO_4)_3$ was reported by [38] and has a completely different structure and topology, which is comprised of NdO_8 polyhedra and SO_4 tetrahedra. Since $Er_2(SO_4)_3$ and $Y_2(SO_4)_3$ have different symmetries and topologies to β-$Yb_2(SO_4)_3$, it would be worthwhile to investigate both $Tm_2(SO_4)_3$ and $Lu_2(SO_4)_3$ to further shed light on the change in these complex topologies and where these changes occur. It will also be interesting to see how many other systematic changes in symmetry and bonding exist within $REE_2(SO_4)_3$ phases, especially within the transition from light-to-heavy REE.

Acknowledgments

Three anonymous reviewers provided helpful comments on the manuscript, which are greatly appreciated. Hao Qi and Mark MacLachlan (Department of Chemistry, UBC) are thanked for providing the TGA data. NSERC Canada is thanked for a Discovery Grant to Mati Raudsepp. Part of this study was funded by the John Jago Trelawney Endowment to the Mineral Sciences Department of the Natural History Museum of Los Angeles County. Developing of the program Jana2006 is permanently supported by Praemium Academiae of the Czech Academy of Sciences.

Appendix A. Supporting information

Supplementary data associated with this article can be found in the online version at doi:10.1016/j.jssc.2011.06.018.

References

[1] N.V. Podberezskaya, S. Borisov, Zh. Struk. Khim. 17 (1976) 186.
[2] L. Hiltunen, L. Niinistoe, Cryst. Struct. Commun. 5 (1976) 561.
[3] I.S. Ahmed Farag, M.A. El Kordy, N.A. Ahmed, Z. Kristallogr. 155 (1981) 165.
[4] H.-U. Hummel, E. Fischer, T. Fischer, P. Joerg, G. Pezzei, Z. Anorg. Allg. Chem. 619 (1993) 805.
[5] M.S. Wickleder, Z. Anorg. Allg. Chem. 625 (1999) 1548.
[6] H. Bartl, E. Rodek, Z. Kristallogr. 162 (1983) 13.
[7] M.S. Wickleder, Chem. Rev. 102 (2002) 2011.
[8] P.C. Junk, C.J. Kepert, B.W. Skelton, A.H. White, Aus. J. Chem. 52 (1999) 601.
[9] E. Gebert Sherry, J. Solid State Chem. 19 (1976) 271.
[10] P. Held, M.S. Wickleder, Acta Crystallogr. E 59 (2003) i98.
[11] A. Dereigne, G. Pannetier, Bull. Soc. Chim. Fr. (1968) 174.
[12] E.B. Hunt, R.E. Rundle, A.J. Stosick, Acta Crystallogr 7 (1954) 106.
[13] L.O. Larsson, S. Linderbrandt, L. Niinistoe, U. Skoglund, Suomen Kemitilehti B 46 (1973) 314.
[14] A. Dereigne, J.M. Manoli, G. Pannetier, P. Herpin, Bull. Soc. Fr. Mineral. Cristallogr. 95 (1972) 269.
[15] S. Bede, Jiegon Huaxue 6 (1987) 70.
[16] Bruker, SAINT, Bruker AXS Inc., Madison, Wisconsin, USA, 2003.
[17] G.M. Sheldrick, SADABS, University of Göttingen, Germany, 2003.
[18] G.M. Sheldrick, Acta Crystallogr. A 64 (2008) 112.
[19] E. Gaudin, V. Petříček, F. Boucher, F. Taulelle, M. Evain, Acta Crystallogr. B 56 (2000) 972.
[20] M.S. Wickleder, Z. Anorg. Allg. Chem. 626 (2000) 1468.
[21] M.I. Aroyo, J.M. Perez-Mato, C. Capillas, E. Kroumova, S. Ivantchev, G. Madariaga, A. Kirov, H. Wondratschek, Z. Kristallogr. 221 (2006) 15.
[22] H.T. Stokes, D.M. Hatch, J.D. Wells, Phys. Rev. B 43 (1991) 11010.
[23] D.M. Hatch, H.T. Stokes, Phys. Rev. B 65 (2001) 014113.
[24] D. Orobengoa, C. Capillas, M.I. Aroyo, J.M. Perez-Mato, J. Appl. Cryst. 42 (2009) 820.
[25] V. Petříček, M. Dušek, L. Palatinus, Jana2006. The Crystallographic Computing System, Institute of Physics, Prague, Czech Republic, 2006.
[26] W.F. Bradley, D.L. Graf, R.S. Roth, Acta. Cryst. 20 (1966) 283.
[27] O. Kamishima, K. Ohta, Y. Chiba, T. Hattori, J. Phys. Condens. Matter 13 (2001) 2455.
[28] D. Zhang, M. Johnsson, R.K. Kremer, Solid State Sci. 12 (2010) 536.
[29] F.C. Hawthorne, S.V. Krivovichev, P.C. Burns, Rev. Mineral 40 (2000) 1.
[30] W.W. Wendtlandt, T.D. George, J. Inorg. Nucl. Chem. 19 (1961) 245.
[31] M.W. Nathans, W.W. Wendtlandt, J. Inorg. Nucl. Chem. 24 (1962) 869.
[32] N. Bukovec, P. Bukovec, J. Siftar, Vestn. Slov. Kem. Drus. 22 (1975) 5.
[33] H.G. Brittain, J. Less-Common Met. 93 (1983) 97.
[34] P.B. Moore, Am. Mineral. 58 (1973) 32.
[35] R.D. Shannon, Acta Crystallogr. 32 (1976) 751.
[36] M.S. Wickleder, Z. Anorg. Allg. Chem. 624 (1998) 1347.
[37] S.P. Sirotinkin, A.N. Pokrovskii, L.M. Kovba, Kristallografiya 26 (1981) 219.
[38] S.P. Sirotinkin, V.A. Efremov, L.M. Kovba, A.N. Pokrovskii, Kristallografiya 22 (1977) 725.